ЖУРНАЛ СТРУКТУРНОЙ ХИМИИ

2013. Том 54, № 6 *Ноябрь – декабрь* *С. 1082 – 1091*

UDC 548.737:547.12:541.67

CONFORMATIONAL VARIABILITY IN A NEW TERPENOID-LIKE BISCHALCONE: STRUCTURE AND THEORETICAL STUDIES

W.B. Fernandes[1], L.A. Malaspina[2], F.T. Martins[3], L.M. Lião[3], A.J. Camargo[1], C. Lariucci[2], C. Noda-Perez[3], H.B. Napolitano[1]

[1]*Ciências Exatas e Tecnológicas, Universidade Estadual de Goiás, 75001-970 Anápolis, GO, Brazil*
E-mail: hamilton@ueg.br
[2]*Instituto de Física, Universidade Federal de Goiás, 74001-970 Goiânia, GO, Brazil*
[3]*Instituto de Química, Universidade Federal de Goiás, 74001-970 Goiânia, GO, Brazil*

Received May, 16, 2012 *Revised September, 25, 2012*

A new terpenoid-like bischalcone (1E,4E)-1-(4-nitrophenyl)-5-(2,6,6-trimethylcyclohex-1-enyl)-penta-1,4-dien-3-one was synthesized from a β-ionone and 4-nitrobenzaldehyde by Claisen—Schmidt condensation reaction and its structure was determined by single crystal X-ray diffraction analysis. Additionally, this compound was featured by powder X-ray diffraction, ^{1}H, ^{13}C NMR and IR spectroscopy techniques. The molecule in the asymmetric unit showed disordered occupancy sites over two positions for the trimethylcyclohexene atoms. These two conformations were related by a rotation of about 180° around the axis of the C—C bond linking the six-membered ring and the olefin carbons. Single-molecule calculations using the DFT method have strengthened this structural finding, since our theoretical approaches also suggest two well-defined conformations of similar energies which resemble the molecular geometries determined by X-ray diffraction. Furthermore, the inspection of the crystal packing revealed that the hydrogen bonding patterns are different for each conformation of the compound reported here.

K e y w o r d s: terpenoid-like bischalcone, X-ray diffraction, disorder modeling.

INTRODUCTION

Chalcones are compounds from either natural sources or synthetic pathways. In plants, these compounds are biosynthesis precursors of flavonoids and isoflavonoids and play several physiological roles such as attraction of pollinators, UV protection, and insect repellence [1—3]. Many biological properties are attributed to chalconas-like as anti-inflammatory [4, 5], anti-mutagenic and antitumoral [1, 6—9], antifungal [10, 11], antimalarial [12—14] and anti-leshimanial effects [12]. Furthermore, chalcones have been subject of several theoretical and experimental studies that aimed the knowledge of their crystal and molecular structures, chemical reactivity, antimicrobial activity, among other applications in the therapy field [11, 15—17]. Chemically, chalcones (1,3-diaryl-2-propen-1-ones) are open-chain flavonoids with two aromatic rings joined by three-carbons from an α—β-unsaturated carbonyl system and can be obtained by Claisen—Schmidt condensation reaction between aldehydes and ketones aromatics in the presence of basic catalysts [3, 4, 11, 15].

Findik *et al.* [18] synthesized sixteen terpenoid-like bischalcones from α or β-ionones and aldehyde derivatives with good yields, thirteen of which were new. All compounds were evaluated against twelve different human pathogenic micro-organims using disk-diffusion technique. Starting from

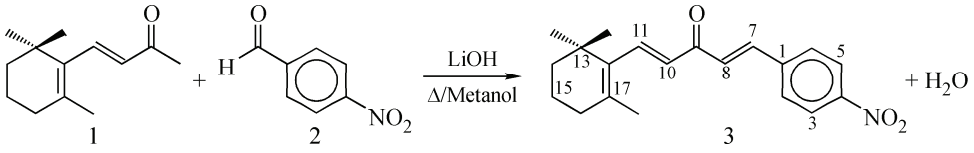

Fig. 1. Synthesis scheme for (**3**) by Claisen-Schimidt condensation reaction

β-ionone (**1**) and 4-nitrobenzaldehyde (**2**), we have synthesized a new terpenoid-like bischalcone (**3**), namely, (1E,4E)-1-(4-nitrophenyl)-5-(2,6,6-trimethylciclohex-1-enyl)-penta-1,4-dien-3-one. This new compound possesses structural analogy with licochalcone A, an oxygenated chalcone isolated from Chinese liquorice roots owning a potent antimalarial activity [14, 19—23].

Besides the synthesis of (**3**), its structure was elucidated by single crystal X-ray diffraction technique which has revealed that 2,6,6-trimethylciclohex-1-enyl moiety is disordered over two positions. In this case, the molecule can possess two well-defined energetically similar conformations which were also approached on single-molecule calculations using the Density Functional Theory (DFT) method [24, 25]. In addition, we describe our results concerning the characterization by complementary methodologies.

EXPERIMENTAL

Synthetic procedure. Compound (**3**) was synthesized by the Claisen—Schmidt condensation reaction between β-ionona (**1**) and p-nitrobenzaldehyde (**2**) in equimolar ratio (2.45 mmol), using $LiOH \cdot H_2O$ as catalyst (2,2 % w/w of β-ionona), as shown in Fig. 1. The reaction mixture was stirred at 55 °C for 90 minutes ending by neutralization with 0.1 M hydrochloric acid solution. The obtained precipitate was filtered and the filtrate was extracted with CH_2Cl_2. Afterward, CH_2Cl_2 was evaporated using rotate evaporator under vacuum at room temperature. The mild yield was 82.2 %. The precipitate formed during evaporation was filtered, washed with ethanol, and air-dried. Crystals of (**3**) were obtained by recrystallization of the initial solid (656.9 mg) in hexane/methanol (1:1) at room temperature.

Crystal structure determination. An orange prism-shaped crystal measuring 0.60×0.55× ×0.20 mm was selected for the X-ray diffraction experiment. The X-ray diffraction intensities for that single crystal were measured using graphite monochromated MoK_α (λ = 0.71073 Å) radiation, in a Bruker Apex II Kappa-CCD diffractometer. The data collecting strategy was calculated setting φ scans and ω scans with κ offsets. The detector was an APEX-II CCD camera on a κ-goniostat. The final unit-cell parameters were based on all collected reflections. The Bruker Apex II software [26] was used for monitoring the diffraction frame acquisition, and the reflections were scaled with the softwares SAINT [27] and SORTAV [28]. No extra absorption correction was applied because the absorption coefficient is negligible for this compound. The structure was solved by direct methods with SIR-92 [29]. All atoms of asymmetric units (except hydrogen) were readily found from the electronic density map constructed by Fourier synthesis. The model obtained was refined by a full-matrix least squares on F^2 with SHELXL-97 [30]. The hydrogen atoms were added to calculated positions and refined with fixed isotropic displacement parameters [$U_{iso}(H) = 1.2U_{eq}$ (C^2_{sp} and C^3_{sp} in methylene groups) or $1.5U_{eq}$ (C^3_{sp} in methyl groups)] using a riding model, with C-H bond lengths of 0.93 Å (those bonded to C^2_{sp}), 0.96 Å (those bonded to C^3_{sp} in methyl groups), or 0.97 Å (those bonded to C^3_{sp} in methylene groups). Anisotropic displacement parameters were used for all non H atoms. The programs MERCURY [31] and ORTEP-3 [32] were used within the WinGX [33] software package to deal with the processed crystallographic data and artwork representations. Crystal data collection and refinement results are presented in Table 1. The CIF file containing full information on the studied structure was deposited with Cambridge Crystallographic Data Centre (CCDC) under deposit code 818053, from where it can be obtained free of charge on request at the following website: www.ccdc.cam.ac.uk/data_request/cif.

Table 1

Crystal data and structure refinement for (**3**)

Empirical formula	$C_{20}H_{23}NO_3$
Molecular weight	325.39
Temperature, K	293(2)
Crystal system	Monoclinic
Space group	$P2_1/c$
Unit cell parameters a, b, c, Å; β, deg.	11.593(2), 11.715(2), 14.202(2); 110.14(5)
Volume, Å^3	1810.9(5)
Z; Density, Mg/m^3	4; 1.19
Absorption coefficient μ, mm^{-1}	0.08
F(000)	696
θ range for data collection, deg.	2.31—25.12
Range of h, k, l	–13/13, –13/13, –16/16
Measured reflections / independent / R_{int}	16991 / 3211 / 0.0608
Completeness for θ_{max}, %	99.7
Data / parameters	2166 / 294
Goodness-of-fit on F^2 (GOOF)	1.042
Final R indices [$I > 2\sigma(I)$]	$R_1 = 0.0501$, $wR_2 = 0.1327$
R indices (all data)	$R_1 = 0.0818$, $wR_2 = 0.1601$
Extintion coefficient	0.008(2)
Largest difference peak and hole, e/Å^{-3}	0.23 and –0.15
Ocupancy factor of conformation 1, %	55.12(2)

During the procedures of structure refinement, disordered sites were found for the atoms of trimethylcyclohexene (hereinafter ring A). Trial refinements have been used with the split-atom approach for these extra sites. From statistical and convergence points of view, the split-atom model with two sites of constrained 53 % and 47 % occupancy factors for these carbons and hydrogens have resulted in the best structural refinement.

Theoretical approaches. The nature of the observed static positional disorder was investigated theoretically within DFT with B3LYP/6-31G* method [34—36]. All the theoretical calculations were carried out using the G09 program package [37] in the gas phase. The structures of both conformers were taken from the X-ray data, but the hydrogen atoms were optimized at the B3LYP/6-31G* level of theory.

Powder X-ray diffraction analysis. Samples of the crystalline material formed on the bottom of glass crystallizer were ground and mounted on a sample holder (grooved glass slide) and exposed to X-ray beam (CuK_α radiation, λ = 1.5418 Å) generated at 40 kV and 30 mA on a *Shimadzu* XRD-6000 diffractometer. The diffractogram was acquired at room temperature under continuous scan mode (scan axis θ—2θ) with scan speed 1.000°/min. Intensity data were measured at each 0.020° in a 2θ range between 5° and 40°. To compare the powder X-ray diffraction profile of (**3**), the CIF file of the structure determined by single crystal, X-ray diffraction technique was used to simulate its theoretical powder X-ray diffractogram with the software MERCURY [31]. Powder X-ray diffraction data were simulated by setting CuK_α beam, 0.020° sampling width, 5—40° 2θ-range and 0.1° 2θ-FWHM.

Additional methodologies for structure characterization. Infrared spectra were recorded as KBr pellets on a FT-IR Perkin-Elmer instrument. The NMR spectra were recorded on a Bruker AVANCE III 500 spectrometer at 298 K and $CDCl_3$ as solvent. The chemical shifts were referenced to the tetramethylsilane peak. Following 1D and 2D pulse sequences from the Bruker user library were used for the NMR experiments:

^{1}H 1D (500.13 MHz): π/2 pulse for ^{1}H 9.9 μs, spectral width 10000 Hz, acquisition time 3.28 s, relaxation delay 1.0 s and the 16 transient free-induction decay was collected with 64 K data points.

HSQC (500.13/125.76 MHz): 2D ^{1}H/^{13}C correlation via double inept transfer, phase sensitive using Echo/Antiecho-TPPI gradient selection, with decoupling during acquisition, using trim pulses in inept transfer: π/2 pulse for ^{1}H 7.4 μs, spectral width in *F*2 10 kHz, acquisition time 0.21 s, relaxation delay 1.0 s, 80 transients per increment, 256 complex data points in *F*1, spectral width in *F*1 25 kHz and linear prediction in *F*1 up to 4 K complex data points.

HMBC (500.13/125.76 MHz): 2D ^{1}H/^{13}C correlation via heteronuclear zero and double quantum coherence, optimised for long-range couplings, no decoupling during acquisition, using gradient pulses for selection: π/2 pulse for ^{1}H 7.4 μs, spectral width in *F*2 10 kHz, acquisition time 0.21 s, relaxation delay 1.0 s, 90 transients per increment, 256 complex data points in *F*1, spectral width in *F*1 28 kHz and linear prediction in *F*1 up to 4 K complex data points.

The data obtained to compound (**3**) were: $[\alpha]_D^{20}$ + 20.6° (*c* 0.002, $CHCl_3$); UV ($CHCl_3$) λ_{max}(log ε) 243 (3.11), 287 (2.71), 363 (2.38) nm; IR (KBr) ν_{max} 2928 (C_{sp}^2—H), 2853 (C_{sp}^3—H), 1735, 1708 (C=O), 1421 (N—O), 891 (Ar) cm^{-1}; ^{1}H NMR ($CDCl_3$, 500 MHz) δ 1.13 (6H, *s*, Me_{13}), 1.51 (2H, *ddd*, *J* = 2.8, 3.2 and 6.1 Hz, H_{14}), 1.65 (2H, *dddd*, *J* = 2.8, 3.2, 6.1 and 6.4 Hz, H_{15}), 1.85 (3H, *s*, Me_{17}), 2.12 (2H, *dd*, *J* = 5.8 and 6.4 Hz, H_{16}), 6.48 (1H, *d*, *J* = 16.1 Hz, H_{10}), 7.11 (1H, *d*, *J* = 15.9 Hz, H_8), 7.57 (1H, *d*, *J* = 16.1 Hz, H_{11}), 7.67 (1H, *d*, *J* = 15.9 Hz, H_7), 7.73 (2H, *d*, *J* = 8.8 Hz, H_3 and H_5), and 8.26 (2H, *d*, *J* = 8.8 Hz, H_2 and H_6); ^{13}C NMR ($CDCl_3$, 125 MHz) δ 18.8 (C_{15}), 21.9 (Me_{17}), 28.9 (Me_{13}), 33.9 (C_{16}), 34.1 (C_{13}), 40.0 (C_{14}), 124.3 (C_2,C_6), 128.9 (C_3,C_5), 129.3 (C_{10}), 129.4 (C_8), 136.5 (C_{12}), 138.0 (C_{17}), 139.7 (C_7), 141.2 (C_1), 144.5 (C_{11}), 148.5 (C_4), and 188.2 (C_9).

RESULTS AND DISCUSSION

Crystallographic analysis. As it can be seen in Fig. 2, an ORTEP-3 [32] representation of the asymmetric unit determined by X-ray diffraction analysis of terpenoid-like bischalcone (**3**), the stereochemistry around both C7=C8 and C10=C11 double bonds is unambiguously described as an (*E*)-configuration. The asymmetric unit of (**3**) consists of a single molecule, exhibiting disordered occupancy sites of the ring A. This disordering is a result of two well-defined molecular conformations. These two conformations are separately shown in Fig. 3.

The bond length and angles between atoms of the two conformations involved with the static disorder are shown in Table 2. The six-membered ring adopts half-chair and twist puckering modes in the conformations with major (conformation 1) and minor (conformation 2) occupancies, respectively. In the conformation 1, C15 lies away from the least-squares plane calculated through the other five cyclic coplanar atoms (r.m.s.d. of the C16′—C17′—C12′—C13′—C14′ fitted atoms is 0.0650 Å) by

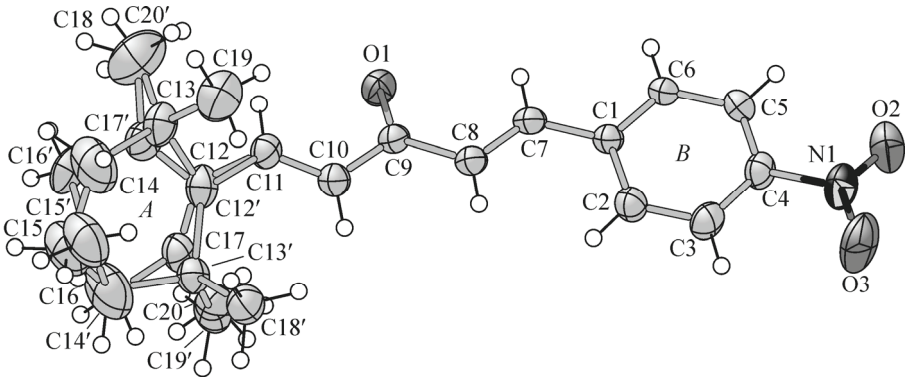

Fig. 2. ORTEP representation with displacement ellipsoids at 30 % probability level of (**3**) after static positional disorder modeled and atom-numbering scheme.
The H atoms are shown as spheres of arbitrary radii

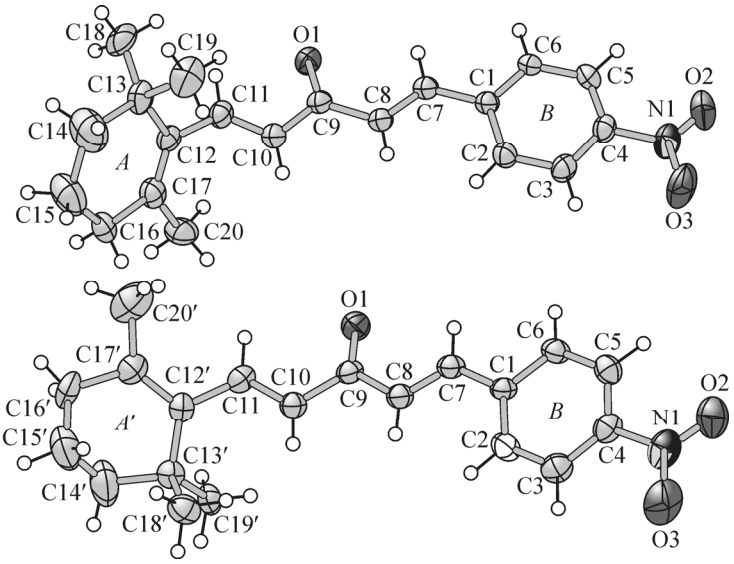

Fig. 3. ORTEP representation with displacement ellipsoids at 30 % probability level of atom arrangement and atom numbering scheme for the two disordered forms obtained of compound (**3**) (conformations 1 and 2).
The H atoms are shown as spheres of arbitrary radii

–0.47(1) Å, while the C14′ and C15′ deviations from the least-squares plane passing through the four coplanar atoms of cyclohexene (r.m.s.d. of the C16′—C17′—C12′—C13′ fitted atoms is 0.0510 Å) are 0.31(2) Å and –0.17(1) Å in the conformation 2. Torsion values also describe both cyclohexene conformations observed. The lowest dihedral angles within the cyclohexene are those on the C12—C13 and C12—C17 bonds in the conformation 1 and on C12′—C17′ in the conformation 2. These torsions, C17—C12—C13—C14 and C16—C17—C12—C13 for the conformation 1 and the C16′—C17′—C12′—C13′ for the conformation 2, measure 6(2)°, –7(2)° and –8(2)°, respectively. Dihedral angles are shown in Table 3 and the intermolecular hydrogen bonds are shown at Table 4.

One more data collection at low temperature of 100 K was undertaken, but no significant improvements of refinement statistics were achieved (100 K cell parameters $a = 11.2795(8)$ Å, $b = 11.5806(8)$ Å, $c = 14.140(1)$ Å, $\beta = 109.6(2)°$ and Final $R_1 = 0.0687$ ($I > 2\sigma(I)$)]. Moreover, the

Table 2

Selected bond lengths (Å) *and angles* (deg.) *for non hydrogen atoms at disorder modeled part of* (**3**)

Bond	Conformation 1	Conformation 2	Angles	Conformation 1	Conformation 2	Angles	Conformation 1	Conformation 2
C11—C12	1.428(1)	1.496(2)	C11—C12—C13	113.2(1)	120.6(1)	C18—C13—C19	112.7(6)	108.5(9)
C12—C17	1.330(2)	1.362(2)	C11—C12—C17	122.5(1)	118.6(1)	C13—C14—C15	121.5(9)	120.2(1)
C12—C13	1.533(2)	1.560(2)	C13—C12—C17	124.1(1)	120.6(1)	C14—C15—C16	116.2(1)	114.8(1)
C13—C14	1.481(1)	1.476(1)	C12—C13—C14	110.5(9)	109.8(1)	C15—C16—C17	112.0(1)	118.2(8)
C13—C19	1.495(8)	1.484(1)	C12—C13—C18	109.2(9)	114.7(1)	C16—C17—C12	121.8(1)	122.4(1)
C13—C18	1.532(1)	1.552(1)	C12—C13—C19	108.9(8)	110.7(1)	C16—C17—C20	114.8(1)	116.1(8)
C14—C15	1.455(1)	1.511(2)	C14—C13—C18	106.4(7)	106.8(1)	C12—C17—C20	123.4(1)	121.5(1)
C15—C16	1.432(2)	1.357(1)	C14—C13—C19	109.1(7)	105.8(1)			
C16—C17	1.558(1)	1.523(1)						
C17—C20	1.555(1)	1.584(1)						

Table 3

Selected dihedral angles (deg.) *for atoms at disorder modeled part of* (**3**)

Dihedral angles	Conformation 1	Dihedral angles	Conformation 2
C10—C11—C12—C13	131.0(8)	C10—C11—C12′—C13′	–27.0(3)
C10—C11—C12—C17	–42.0(3)	C10—C11—C12′—C17′	161.9(2)
C11—C12—C13—C18	61.2(2)	C11—C12′—C13′—C18′	80.0(2)
C11—C12—C13—C19	–54.2(2)	C11—C12′—C13′—C19′	–43.0(3)
C11—C12—C17—C20	–8.0(3)	C11—C12′—C17′—C20′	–6.0(3)
C13—C12—C17—C20	179.8(2)	C13′—C12′—C17′—C20′	–177.9(2)
C17—C12—C13—C18	–126(2)	C17′—C12′—C13′—C18′	–109.0(2)
C17—C12—C13—C19	119.1(2)	C17′—C12′—C13′—C19′	128.2(2)
C15—C16—C17—C20	–176.0(2)	C15′—C16′—C17′—C20′	–152.4(2)
C12—C13—C14—C15	19(1)	C12′—C13′—C14′—C15′	–37(1)
C13—C14—C15—C16	–44(2)	C13′—C14′—C15′—C16′	44(2)
C14—C15—C16—C17	40(2)	C14′—C15′—C16′—C17′	–29(1)
C15—C16—C17—C12	–16(2)	C15′—C16′—C17′—C12′	13(2)
C16—C17—C12—C13	–7(2)	C16′—C17′—C12′—C13′	–8(2)
C17—C12—C13—C14	6(2)	C17′—C12′—C13′—C14′	19(2)

X-ray diffraction measurement at low temperature revealed that unit cell parameters, crystal packing and molecular backbones do not vary significantly with the temperature in this range (Table 1). Therefore, these structure determinations at 293 K and 100 K demonstrate that no solid-solid phase transformation occurs between the evaluated temperatures.

The main difference between the molecular conformations of (**3**) is in the C11—C12 bond axis rotation, resulting in different orientations for ring A. The values of the C10—C11—C12—C13 and C10—C11—C12—C17 dihedral angles change between the two conformations by about 158° and 204°, respectively, while the values of the other torsions do not quite differ for the two conformations (Table 3). These two conformations are related to different patterns of intermolecular interactions. All hydrogen bonds contributing to the crystal assembly of (**3**) are non-classical, wherein C—H groups are hydrogen bonding donors to both nitro and carbonyl oxygens (Figs. 4—6). The conformation 2 is stabilized by three hydrogen bonds, whereas the conformation 1 is stabilized by only two hydrogen bonds

Table 4

Hydrogen bonding of two conformations obtained for compound (**3**)

D—H···A	D—H, Å	D···A, Å	H···A, Å	D—H···A, deg.
Conformation 1				
C8—H8···O3^{i}	0.93	3.392(4)	2.56	150
C16—H16a···O1^{ii}	0.97	3.355(3)	2.55	141
Conformati on 2				
C8—H8···O3^{iii}	0.93	3.394(3)	2.56	150
C14′—H14d···O1^{i}	0.97	3.400(2)	2.48	159
C19′—H19d···O2^{ii}	0.96	3.570(3)	2.62	170

Symmetry operations: (i) *x*, 1/2–*y*, –1/2+*z*; (ii) *x*, –1/2–*y*, –1/2+*z*; (iii) *x*, –1/2–*y*, –1/2–*z*.

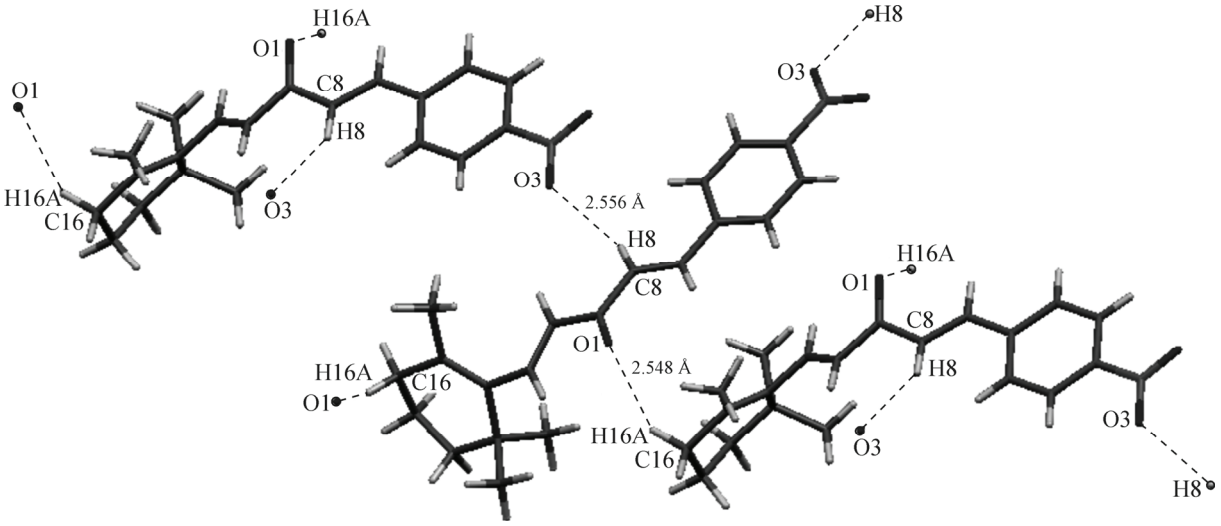

Fig. 4. Non classical H bonds of conformation 1 for the compound (**3**)

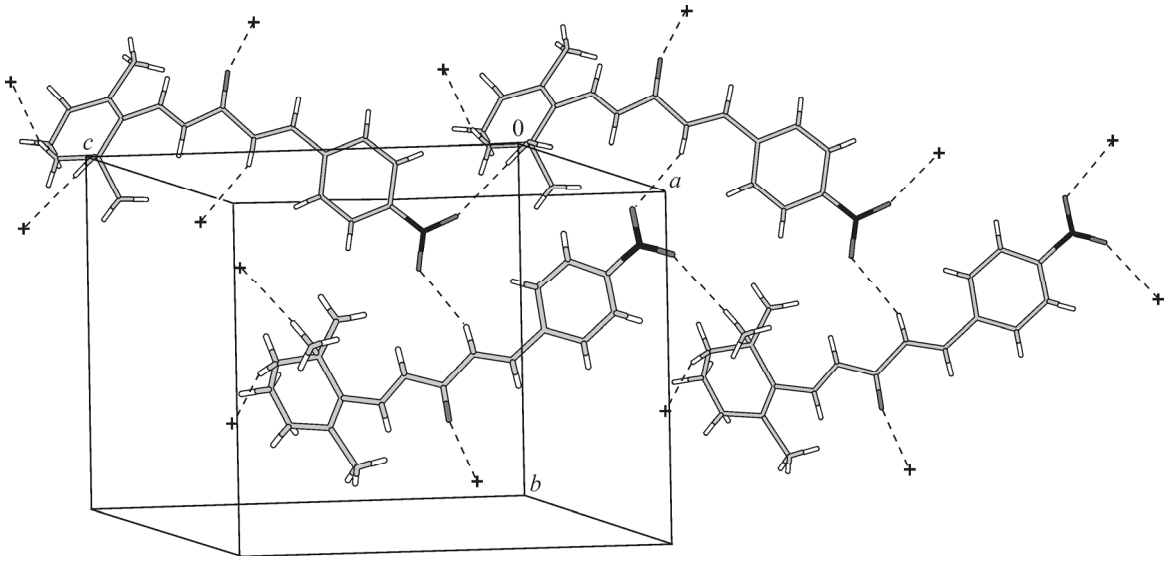

Fig. 5. Non classical H bonds of conformation 2 for the compound (**3**)

contributing to the energy barrier found. The calculated energy difference between the conformers (Fig. 3) is only 0.10 kcal/mol. This result shows that the two conformers are energetically very similar and, at room temperature, the two conformations are equally populated. Fig. 7 shows the structure overlay of conformers of (**3**) for both calculated (B3LYP/6-31G*) and experimental geometric parameters.

Additional analyses. The ^{1}H NMR spectrum displayed two doublets at δ 7.73 and 8.26 (J = = 8.8 Hz, H_2, H_3, H_5 and H_6), with 2 hydrogen each signal, typical of *p*-substituted aromatic ring. Two olefinic systems in *trans* configuration were characterized by doublets at δ 6.48 (J = 16.1 Hz, H_{10}), 7.57 (J = 16.1 Hz, H_{11}), 7.11 (J = 15.9 Hz, H_8), and 7.67 (J = 15.9 Hz, H_7). These data associated with complex signals at δ 1.51 (ddd, J = 2.8, 3.2, 6.1 Hz, H_{14}), 1.65 (dddd, J = 2.8, 3.2, 6.1, 6.4 Hz, H_{14}), and 2.12 (dd, J = 5.8, 6.4 Hz, H_{16}), and three methyl groups at δ 1.13 (6H) and 1.85 (3H), referring to six-membered unsaturated and trimethylated ring, leading to a proposed structure comprising one chalcone and one retinoid units. This proposes were reinforced by ^{13}C data obtained through HSQC and HMBC, wherein olefinic hydrogen correlates to carbonyl group and rings.

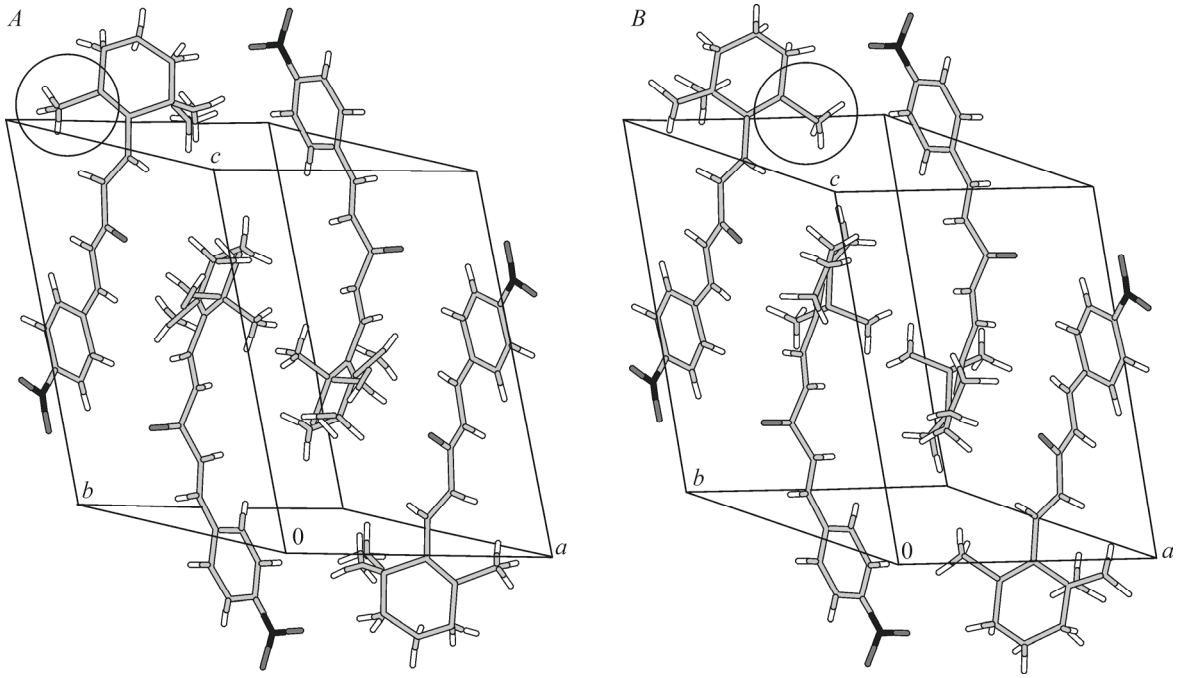

Fig. 6. Molecular packing of the conformers 1 and 2 showing the difference between the two conformations in the molecular packing

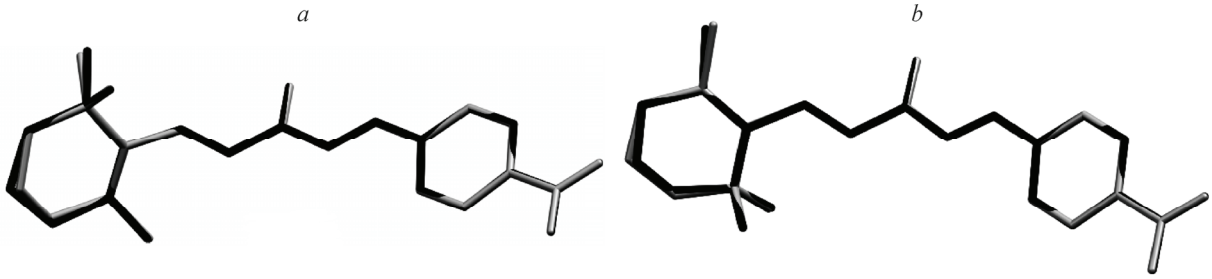

Fig. 7. Structure overlay of conformers of (**3**) for both calculated (gray) and experimental (black) geometric parameters.
(*a*) Conformation 1 and (*b*) conformation 2

To determine the solid-state phase of the crystalline material obtained after synthesizing (**3**), we have compared the theoretical powder X-ray diffraction peak positions and intensities calculated from its crystal structures to the corresponding experimental diffractogram as shown in Fig. 8. All peaks in the experimental X-ray diffractogram of ground samples of crystalline material formed after the crystallization procedure were observed in the calculated X-ray diffractogram from the single crystal structure of (**3**) (data collected at 293 K). Therefore, we can state that the obtained material has no extra crystalline phase.

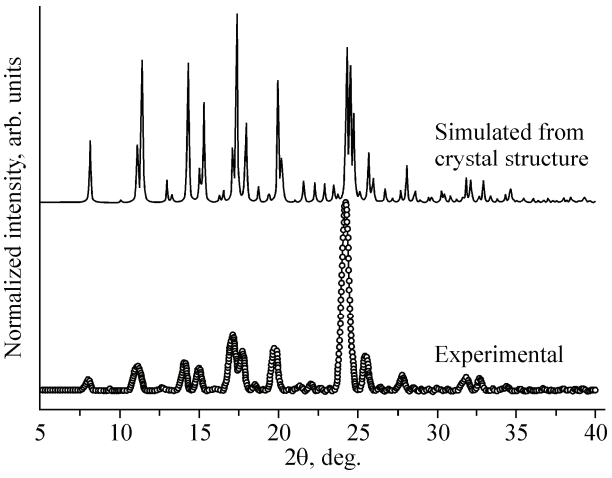

Fig. 8. Comparation of theoretical and experimental powder diffractogram for compound (**3**)

Likewise, no broad hump was observed in the experimental X-ray diffraction profile, allowing us to conclude that there are not amorphous solids together with the crystalline material of (**3**). To notice, preferred orientation effects were observed in the experimental powder X-ray measured diffractogram. The X-ray diffraction intensities in the simulated and the experimental diffractograms do not totally agree because of the preferred orientation of the Bragg (3 0 0) reflection (in 24.5° in 2θ).

CONCLUDING REMARKS

As it can be seen in the X-ray data, the packing of both conformers are equally favorable. From these results we can hypothesize that the observed disorder appears from (i) energetic similarity between both conformers and (ii) similar probability of packing during the crystal growth process.

Acknowledgments. The authors gratefully acknowledge the financial support of Coordenação de Aperfeiçoamento de Pessoal de Nível Superior (CAPES), Brazil. We also thank Dr. Charles H. Lake for X-ray data collection during the 2009 American Crystallographic Association (ACA) Summer Course in Small Molecule Crystallography, and Dr. Julio Zukerman Schpector of Universidade Federal de São Carlos (UFSCar) for fruitful discussions.

REFERENCES

1. *Echeverria C., Santibañez J.F., Donoso-Tauda O., Escobar C.A., Ramirez-Tagle R.* // Int. J. Mol. Sci. – 2009. – **10**. – P. 221.
2. *Eddarir S., Cotelle N., Bakkoura Y., Rolando C.* // Tetrahedron Lett. – 2003. – **44**. – P. 5359.
3. *Climent M.J., Corma A., Iborra S., Velty A.* // J. Catal. – 2004. – **221**. – P. 474.
4. *Nowakowska Z.* // Eur. J. Med. Chem. – 2007. – **42**. – P. 125.
5. *Paulino N., Rodrigues N.C., Pardi P.C., Suárez J.A.P.Q., Santos R.P., Scremin A., Vogel C., Feist H., Michalik D.* // Bioorg. Med. Chem. – 2009. – **17**. – P. 4290.
6. *LeBlanc R., Dickson J., Brown T., Stewart M., Pati H.N., VanDerveer D., Arman H., Harris J., Pennington W., Holt H.L., Lee M.* // Bioorg. Med. Chem. – 2005. – **13**. – P. 6025.
7. *Liu X., Go M.L.* // Bioorg. Med. Chem. – 2007. – **15**. – P. 7021.
8. *Nam N.H., Kim Y., You Y.J., Hong D.H., Kim H.M., Ahn B.Z.* // Eur. J. Med. Chem. – 2003. – **38**. – P. 179.
9. *Cabrera M., Simoens M., Falchi G., Lavaggi M.L., Piro O.E., Castellano E.E., Vidal A., Azqueta A., Monge A., Ceráin A.L., Sagrera G., Seoane G., Cerecettoa H., González M.* // Bioorg. Med. Chem. – 2007. – **15**. – P. 3356.
10. *Batovska D., Parushev S., Stamboliyska B., Tsvetkova I., Ninova M., Najdenski H.* // Eur. J. Med. Chem. – 2009. – **44**. – P. 2211.
11. *Batovska D., Parushev S., Slavova A., Bankova V., Tsvetkova I., Ninova M., Najdenski H.* // Eur. J. Med. Chem. – 2007. – **42**. – P. 87.
12. *Liu M., Wilairat P., Croft S.L., Tan A.L.C., Goa M.L.* // Bioorg. Med. Chem. – 2003. – **11**. – P. 2729.
13. *Larsen M.* // Bioorg. Med. Chem. Lett. – 2005. – **15**. – P. 4858.
14. *Charris J.E., Domínguez J.N., Gamboa N., Rodrigues J.R., Angel J.E.* // Eur. J. Med. Chem. – 2005. – **40**. – P. 875.
15. *López S.N., Castelli M.V., Dominguez J.N., Zacchino S.A., Lobo G., Charris-Charris J., Cortés J.C.G., Ribas J.C., Devia C., Rodriguez A.M., Enriz R.D.* // Bioorg. Med. Chem. – 2001. – **9**. – P. 1999.
16. *Yang W., Wang L., Zhang D.* // J. Chem. Crystallogr. – 2006. – **36**. – P. 195.
17. *Shettigar V., Patil P.S., Naveen S., Dharmaprakash S.M., Sridhar M.A., Prasad S.J.* // J. Cryst. Growth. – 2006. – **295**. – P. 44.
18. *Findik E., Dingil A., Karaman I., Ceylan M.* // Synthetic Commun. – 2009. – **39**. – P. 4362.
19. *Zhou J., Geng J., Wu J.H.* // Bioorg. Med. Chem. Lett. – 2009. – **19**. – P. 1183.
20. *Zhou J., Geng J., Wu J.H.* // Invest. New Drugs. – 2010. – **28**. – P. 291.
21. *Chen M., Zhai L., Christensen S.B., Theander T.G., Kharazmi A.* // Antimicrob Agents Chemother. – 2001. – **45**. – P. 2023.
22. *Valla A., Valla B., Cartier D., Guillou R., Labia R., Florent L., Charneau S., Schrevel J., Portier P.* // Eur. J. Med. Chem. – 2006. – **41**. – P. 142.
23. *Costa S.L.* // J. Med. Biol. Sci. – 2004. – **3**. – P. 224.
24. *Müller P.* // Crystallogr. Rev. – 2009. – **15**. – P. 57.

25. *Müller P., Irmer R.H., Spek A.L., Schneider T.R., Sawaya M.R.* Crystal structure refinement: a crystallographer′s guide to SHELXL. – New York: Oxford University Press, 2006.
26. Bruker APEX2 (version 2.1-4) Bruker AXS, Inc., Madison, Wiscosin, USA, 2007.
27. Bruker SAINT (version 7.34A) Bruker AXS, Inc., Madison, Wiscosin, USA, 2007.
28. *Blessing R.H.* // Acta Crystallogr. A. – 1995. – **51**. – P. 33.
29. *Altomare A.A., Cascarano G., Giacovazzo C., Guagliardi A.* // J. Appl. Crystallogr. – 1993. – **26**. – P. 343.
30. *Sheldrick G.M.* // Acta Crystallogr. A. – 2008. – **64**. – P. 112.
31. *Macrae C.F., Edgington P.R., McCabe P., Pidcock E., Shields G.P., Taylor R., Towler M., van De Streek J.* // J. Appl. Crystallogr. – 2006. – **39**. – P. 453.
32. *Farrugia L.J.* // J. Appl. Crystallogr. – 1997. – **30**. – P. 565.
33. *Farrugia L.J.* // J. Appl. Crystallogr. – 1999. – **32**. – P. 837.
34. *Becke A.D.* // J. Chem. Phys. – 1993. – **98**. – P. 5648.
35. *Lee C., Yang W., Parr R.G.* // Phys. Rev. B. – 1998. – **37**. – P. 785.
36. *Miehlich B., Savin A., Stoll H., Preuss H.* // Chem. Phys. Lett. – 1989. – **157**. – P. 200.
37. *Frisch M.J., Trucks G.W., Schlegel H.B. et al.* GAUSSIAN 09 Revision A02. Gaussian, Inc., Wallingford, CT, 2009.